Chemical Geology 511 (2019) 28–41

Contents lists available at ScienceDirect

Chemical Geology

journal homepage: www.elsevier.com/locate/chemgeo

Liquid immiscibility in the CaF_2-granite system and trace element partitioning between the immiscible liquids

Longbo Yang*, Vincent J. van Hinsberg

Department of Earth and Planetary Sciences, McGill University, 3450 Rue University, Montreal H3A0E8, Canada

ARTICLE INFO

Editor: D.B. Dingwell

Keywords:
Liquid immiscibility
CaF_2-granite system
Trace element partitioning
Rare earth elements

ABSTRACT

The recent discoveries of Ca-fluoride melt in magmatic systems, especially in peralkaline granites with rare earth element enrichment, has raised questions about the presence and nature of liquid immiscibility in CaF_2-granite systems, as well as the partitioning behavior of trace elements between such immiscible liquids. We have experimentally explored the immiscibility in this system using natural granite-fluorite starting materials at fast-and slow-cooling rates, temperatures from 500 °C to 1200 °C and 1 atmosphere pressure. Our experiments confirm the presence of a miscibility gap in the CaF_2-granite system over a wide range of temperatures. The two immiscible liquids are a mafic fluorosilicate melt (*fm*) with high CaO and F and a felsic oxysilicate melt (*sm*) with high SiO_2 and alkalis. Immiscibility is encountered when the bulk F-content exceeds approximately 4.4 wt% at 1200 °C and then rapidly decreases to only 0.75 wt% at low temperature (below 900 °C). This indicates that calcic magmas are able to evolve to the liquid immiscibility domain by the residual enrichment of fluorine resulting from fractional crystallization, and that liquid immiscibility should be common. The peritectic reaction *fm* = *sm* + fluorite removes the fluorosilicate liquid around 600 °C and could explain the absence of fluorosilicate observations in natural granites. The compositions of the liquids in fast-cooling experiments show a significantly larger miscibility gap which is characterized by, compared to slow-cooling runs, similar *sm* compositions but higher Ca and F content in *fm*. This difference is caused by suppression of fluorite nucleation and is interpreted as a metastable extension of the high temperature liquid immiscibility. Immiscibility results in strong fractionation of trace elements which is primarily governed by melt structure and the ionic potential (Z/r) of the elements. The behavior of trace elements can be categorized into three groups: 1. Network formers (Si, Al, Ga, Pb, B) partition into the oxysilicate melt; 2. The partitioning of the alkalis and alkali earths is strongly dependent on the ionic potential, with the partitioning coefficients ($D^{fm}/_{sm}$) in the order $D_{Cs} < D_{Rb} < D_K < D_{Na} < D_{Li} < D_{Ba} < D_{Sr} < D_{Ca} \leq D_{Mg}$; 3. High field strength elements (Ti, Zr, Hf, Nb, Ta, Th, U) and rare earth elements (REE) strongly partition into the fluorosilicate melt. The D values vary with the size of the miscibility gap, which is in turn controlled by temperature with more pronounced fractionation as the miscibility gap widens. The fluorosilicate melt effectively sequesters the REE especially at the lower temperatures relevant for granite magmatism and, given its higher density and lower viscosity compared to the coexisting oxysilicate melt, fractionates the REE from the host silicate melt, suggesting a potential REE-mineralising process.

1. Introduction

Liquid immiscibility in fluoride-silicate systems has been extensively studied since the 1950s when the phase relations and thermodynamic properties of the CaF_2-SiO_2 system were experimentally explored for the first time (Berezhnoi, 1951) owing to its industrial utilization in metallurgy and ceramic production (e.g. Hillert, 1964; Ueda and Maeda, 1999). In geology, fluoride-silicate liquid immiscibility received the attention of experimental petrologists as a potential mechanism for generating elevated fluorine contents in highly evolved granitic and rhyolitic magmas (Dolejš and Baker, 2007a, b). Despite the experimental work on multicomponent fluoride-silicate systems, the presence and location of any miscibility gaps in these systems are still debated (see Dolejš and Baker, 2007a; Jung et al., 2015). Furthermore, most experiments have been performed in granite–alkali fluoride systems because high fluorine concentrations are more commonly found in alkaline-peralkaline granites and associated pegmatites (Kogarko and Krigman, 1970; Gramenitskiy and Shchekina,

* Corresponding author.
E-mail address: longbo.yang@mail.mcgill.ca (L. Yang).

https://doi.org/10.1016/j.chemgeo.2019.02.017
Received 11 September 2018; Received in revised form 14 January 2019; Accepted 10 February 2019
Available online 15 February 2019
0009-2541/

1994). However, only rare evidence in the form of alkali-fluoride glass (e.g. as melt inclusions) has been reported (Andreeva et al., 2007; Solovova et al., 2010), possibly because of issues with trapping such inclusions (Roedder, 1992), the difficulty of preserving these during later hydrothermal processes and sample preparation because of the high solubility of NaF and KF in aqueous solutions, or even a lack of effort to recognize and identify such inclusions (Kamenetsky et al., 2004; Potter et al., 2017).

Less attention has been paid to calcic systems. This is somewhat surprising given that fluorite (CaF_2) is the most common fluoride mineral in magmatic systems (Dolejš and Baker, 2006) and binary or ternary systems involving CaF_2 and SiO_2 are known to produce liquid immiscibility (Hillert, 1964; Jung et al., 2015; Ueda and Maeda, 1999). Recently, fluorosilicate melt has been discovered in nature, co-trapped with silicate melt in melt inclusions in an alkaline granite (Peretyazhko et al., 2007; Vasyukova and Williams-Jones, 2014, 2016), as part of the groundmass in carbonatitic magmas (Potter et al., 2017), and as melt pockets in mantle xenoliths (Klemme, 2004). These examples represent the first direct evidence of the occurrence of immiscible fluoride melt in nature. It also suggests that melt immiscibility associated with CaF_2 may play an important role in the chemical evolution of calcic granitic systems and the behaviour of their trace elements (see Vasyukova and Williams-Jones, 2014, 2016). Even so, the interpretation of these natural occurrences as melt immiscibility is still debated (Dawson et al., 1995; Dolejš, 2005; Klemme, 2005; Potter et al., 2017), in part because direct experimental evidence for immiscibility in these systems is lacking. The experimental studies so far conducted for CaF_2 – silicate (Webster et al., 1998; Veksler, 2004; Veksler et al., 2012) are all in limited chemical systems that restrict their extrapolation to geologically relevant compositions.

Immiscible melts are commonly characterized by strongly contrasting trace element preferences, leading to high inter-melt element partition coefficients. This is particularly true for carbonatite-silicate and sulphate-silicate systems where favorable partitioning of economically interesting elements into molten salt could potentially be an important mechanism for ore-element sequestration and concentration (e.g. Fleet et al., 1991; Peach et al., 1994; Martin et al., 2013). Vasyukova and Williams-Jones (2014, 2016) show strong REE-partitioning between silicate and fluoride immiscible melts in their natural samples, and they suggest that fluoride-silicate melt separation could be an important, possibly dominant process for the initial enrichment of REE in F-rich alkaline silicate systems. The experimental findings of Veksler (2004) and Veksler et al. (2012) are consistent with the behavior of the REE in these natural rocks, but their experimental compositions and temperature conditions are too different to be directly applied to natural systems.

To address the debate surrounding the fluorosilicate glass inclusions in nature, and to evaluate the potential significance of F-induced liquid immiscibility on REE-behaviour in calcic magmatic systems, we have conducted a series of experiments in the granite-CaF_2 system over a range of temperature conditions. We used a natural granite mixed with fluorite to explore liquid immiscibility in this system and generate partition coefficients for a suite of trace elements with particular focus on the rare earth elements for the potential implications in REE-ore formation.

2. Experimental and analytical method

2.1. Description of experiments

Exploratory experiments were conducted to find the optimal starting composition for generating liquid immiscibility in the CaF_2-granite system (Table 1). To simulate compositions of direct relevance to nature, the starting mixtures were prepared from granite mixed with calcium fluoride. The granite sample is the hypersolvus granite (for composition see Table 2) in the Strange Lake pluton, Canada, for which fluoride-silicate melt immiscibility has been described (see Vasyukova and Williams-Jones, 2016). The source of calcium fluoride is a natural, transparent and colorless fluorite from Alfa Aesar (inventory code 44373). Small amounts (< 1 wt%) of boron, as trace-metal grade boric acid, were added to some of the experiments as a fluxing agent to mimic the effect of the water present in natural systems, because like water, boron lowers the liquidus (e.g. Chorlton and Martin, 1978) and reduces melt viscosity (e.g. Dingwell et al., 1992). Starting compositions were ground in an agate mortar under ethanol into a fine powder and sealed in welded quartz tubes, which were heated in a box furnace at 1200 °C for 5 h at least once. All exploratory experiments are conducted anhydrous at 1200 °C, at 1 atm pressure with different CaF_2: granite ratios to locate the immiscibility field (Table 1). The optimal starting composition P1 as determined from these experiments was used for the subsequent liquid immiscibility experiments with a smaller set of experiments using composition P2.

2.1.1. Main experiments

A series of experiments was carried out to systematically explore the silicate-fluoride melt immiscibility field at temperatures from 1200 to 500 °C, and to determine the melt/melt partition coefficients for a wide range of trace elements. The P1 starting material used in this temperature series was similarly prepared from granite and fluorite starting materials, mechanically mixed by grinding in an agate mortar under ethanol and fused at 1200 °C for > 5 h. It was subsequently re-ground and this fusion procedure was repeated three times to guarantee homogeneity of the starting material. About 0.35 wt% boron in the form of boric acid was added to the CaF_2-granite mixture, as well as trace elements in the form of ICP-MS single element nitrate standard solutions to ensure that the concentrations of alkaline and alkaline earth elements were above 100 ppb, and rare earth elements above 10 ppm to facilitate subsequent analyses. The doped starting material was heated to 450 °C to dry the solutions and denitrify the trace elements, and then fused again at 1200 °C for 4 h. Composition P2 was not doped with trace elements and acted to confirm the phase relations obtained from composition P1. The starting compositions for P1 and P2 are given in Table 2.

Experiments were performed at ambient pressure and at temperatures from 1200 to 500 °C in a box furnace. Temperature was controlled by a Eurotherm PIDU controller and independently verified using a type-K thermocouple which shows that temperature was maintained to within ± 5 °C. Charges of 100 to 250 mg of starting material were sealed in quartz tubes and placed into the furnace at 1200 °C at which temperature they were kept for 5 to 6 h. They were then cooled down to run temperature. Two series of experiments with different cooling rates were performed to study its impact on immiscibility textures and phase separation; one series at a fixed cooling rate of 6 °C per hour and the other dropping down to run temperature within 1 or 2 h. The temperature range for slow-cooling experiments is 700 to 1100 °C, and for fast-cooling experiments 500 °C to 1100 °C. No cooling was involved in the experiment at 1200 °C so the data for this experiment were used for both series in the discussion. We did not run any experiments above 1200 °C to avoid weakening and failure of the quartz tubes. A summary of the experimental conditions is given in Table 3 and shown in Fig. 1.

After the experiments, run products were quenched within a few seconds by dropping the quartz tubes into olive oil. The run products were then mounted in epoxy, polished, imaged using reflected-light microscopy and back-scattered electron imaging, and analyzed by electron microprobe for major elements and laser ablation ICP-MS for trace elements.

2.2. Electron microprobe analyses

Major components were analyzed using a JEOL 8900RL electron microprobe. Analyses were performed using wavelength-dispersive spectrometry (WDS) with a 4 nA beam current and accelerating voltage

Table 1
Run conditions for the exploratory experiments. The starting mixture ratios are by weight. The difference between the initial F content and that measured is due to fluorine loss during the fusion process.

Experiment number	Starting mixture ratio	Measured fluorine content	Run temperature (°C)	Duration (hours)	Boron added?	Immiscible liquids
ME-3b	CaF_2-granite (1:3)	6 wt%	1200	75	Yes	Yes
ME-4a	CaF_2-granite (1:5)	4 wt%	1200	90	Yes	Local
ME-5	CaF_2-granite (1:6)	3.5 wt%	1200	72	Yes	Local
ME-6a	CaF_2-granite (1:8)	2.6 wt%	1200	72	Yes	No
ME-6b	CaF_2-granite (1:10)	2.2 wt%	1200	72	Yes	No
ME-7b	CaF_2-granite (1:11)	2 wt%	1200	48	Yes	No
ME-30a	CaF_2-granite (1:3)	~10 wt%	1200	5	No	Yes

Table 2
Major element compositions of the starting materials P1 and P2 and the starting granite sample (in wt%). Compositions for the starting materials are normalized to 100 wt%. n.d. stands for not determined. The granite composition is from Olga Vsyukova (personal communication).

	Granite	P1	P2
SiO_2	70.90	58.22	69.64
Al_2O_3	11.53	7.97	8.30
Fe_2O_3 (total)	5.09	3.14	3.18
CaO	0.90	19.19	7.62
Na_2O	4.94	3.16	3.03
K_2O	4.74	2.90	3.47
TiO_2	0.35	0.24	0.25
B_2O_3	n.d.	1.13	1.12
ZrO_2	0.67	0.44	0.44
F	0.46	6.23	5.11
L.O.I.	1.13	n.d.	n.d.
Total	100.71	102.62	102.15
−O=2F	0.19	2.62	2.15
Total (−O=2F)	100.52	100.00	100.00

Table 3
Run conditions and phase assemblage of the run products. For fast cooling experiments, cooling rate was not measured, but the final temperature was reached within 2 h for all experiments. The duration of an experiment consists of the length of time at run temperature, time of cooling (for slow-cooling experiments) and time at 1200 °C before quenching. Abbreviations for phases: *fm* = fluorosilicate melt; *sm* = oxysilicate melt; *fl* = fluorite.

Run	Starting composition	T	Cooling rate (°C/h)	Duration	Phase composition
ME-14	P1	1200	N/A	5	fm + sm
ME-8	P1	1200	N/A	72	fm + sm
ME-27a	P1	1100	6	72 + 16.7 + 6	fm + sm + fl
ME-9c	P1	1000	6	72 + 33.3 + 2	fm + sm + fl
ME-24	P1	900	6	72 + 50 + 5	fm + sm + fl
ME-15d	P1	800	6	72 + 66.7 + 5	fm + sm + fl
ME-32a	P1	700	6	73 + 83.3 + 5	fm + sm + fl
ME-29	P1	1100	Fast	72 + 6	fm + sm + fl
ME-40	P1	1000	Fast	72 + 6	fm + sm + fl
ME-20	P1	900	Fast	92 + 6	fm + sm + fl
ME-23	P1	800	Fast	74 + 6	fm + sm + fl
ME-16b	P1	700	Fast	81 + 6	fm + sm + fl
ME-21b	P1	600	Fast	280 + 5	fm + sm + fl
ME-13d	P1	600	Fast	72 + 5	fm + sm + fl
ME-18b	P1	500	Fast	77 + 5	fm + sm + fl
ME-9b	P2	1000	6	72 + 33.3 + 2	fm + sm + fl
ME10b	P2	900	Fast	204 + 3	fm + sm + fl
ME-15b	P2	800	6	72 + 66.7 + 5	fm + sm + fl
ME-16a	P2	700	Fast	81 + 6	fm + sm + fl
ME-22	P2	600	12	480 + 50 + 3	sm + fl

of 15 kV. The EMP was calibrated on natural peralkaline obsidian glass Ke-12 (Na and K) (Stix et al., 1995), two natural basaltic glasses BJDF (Ca, Mg and Fe) and Bmak (Ti, Al and Si) from Smithsonian Institute, and synthetic glass SGT4 (F). Thallium acid phthalate (TAP) crystal was used to analyze fluorine to avoid Fe interference. Measurement times

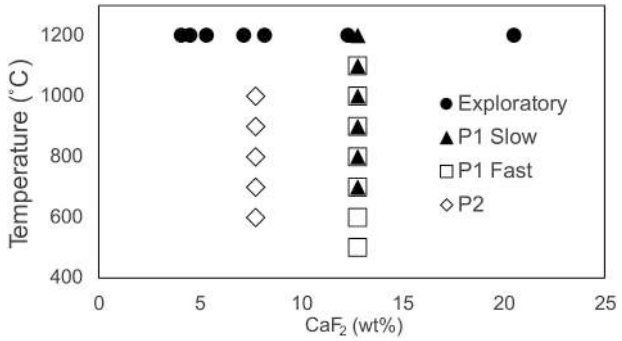

Fig. 1. A schematic representation of the starting compositions and conditions of experiments referred to in this study.

on peak were 20 s for Na, Mg, Al and Si, 30 s for K, Ca and Fe, 40 s for Mn and Ti, and 60 s for F. Measurement times on background were half of those on peak. Two natural peralkaline obsidian glasses KN-9 and UTR, natural metaluminous obsidian glass UDM-1 (Stix et al., 1995), and NIST SRM 610 were used as secondary reference materials to check for bias and drift (none were found). At least five analyses were performed on each phase to assess the homogeneity in major-element composition and obtain statistically representative means. Different beam sizes from 3 to 50 μm were used depending on the size of individual phases. Monitoring the Na_2O counts over the counting time shows no significant Na loss when using a 3 μm beam size. The EMP was calibrated at 50 μm and 10 μm to account for the range of beam sizes used during analysis, but no significant difference in concentration was observed when using these two calibrations for a given material.

2.3. Laser ablation ICP-MS analyses

Trace elements in the run products were analyzed by laser ablation ICP-MS using a NewWave 213 nm Nd-YAG laser ablation system combined with a Thermo Finnigan iCapQc quadrupole ICP-MS. Analyses were done with a laser fluence of 6 J/cm^2, a laser repetition rate of 10 Hz, and counting times of 30 s on background, 60 s on sample and 30 s washout. Laser spot sizes of 12, 16, 20, 30 and 40 μm were used to match the size of run-product phases. Before each analysis, a 1-s pre-ablation with a spot size of 120 μm and 30 s of washout was performed to clean the sample surface. The reference material NIST SRM 610 was used as the external calibration standard and bracketed each set of analyses. It was measured at the same range of laser spot sizes as used for the samples. Concentrations of Al as determined by electron-microprobe were used as an internal reference to correct for differences in ablation behavior between standard and samples. Reference glasses BCR-2G and GSD-1G are used as secondary standards to examine the accuracy of the analyses, using the reference values from (Jochum and Stoll, 2008). Data accuracy is better than 20% relative for all elements except for Y (−24%), Dy (−23%), Tm (−22%), Yb (−22%). Data reduction, as well as drift correction, was conducted in software package Iolite version 2.5 (Hellstrom et al., 2008).

2.4. Quantification of Laser ablation ICP-MS analyses

Experiments ME-8 (1200 °C), ME-27a (1100 °C slow-cooling), ME-9C (1000 °C slow-cooling) and ME-29 (1100 °C fast-cooling) have good phase separation and the individual globules of immiscible melt are large enough for laser spot sizes of 30 or 40 µm in diameter so that data for these samples can be processed using traditional data reduction techniques (see Longerich et al., 1996). The globules of immiscible melts in run products from experiments performed at other temperatures are too small in size for even a 12 µm spot to obtain a single-phase signal. In these cases, ablation includes the target material plus its host, and the mixed analysis needs to be de-convoluted. This is achieved using the method set out in Yang et al. (2018), which is based on linear regression of variable mixtures of target and host with end-members constrained from major elements using EMP analyses. Yang et al. (2018) developed this method for the specific samples presented here, and tests using sample ME-8 showed an accuracy within ± 15% relative when comparing the traditional data quantification method to the linear regression method and may in some cases provide better data than traditional analyses (see Yang et al. 2018 for details). This approach was unfortunately not applicable to the slow-cooling experiments from 900 to 700 °C, because the mixtures contain a third phase, fluorite, which prevents an accurate deconvolution. Given this, no trace element data could be obtained for these experiments.

3. Results

3.1. Run products and textures

Typical run products of the exploratory experiments are shown in Fig. 2. Experiments using starting mixtures with low CaF_2/granite ratios (ME-6a, 6b, 7b) do not exhibit evidence for melt immiscibility and show only a homogeneous fluorine-bearing silicate glass. The experiments with moderate CaF_2/granite ratios (ME-4a, 5) show only local liquid immiscibility with the majority of the run products a fluorine-bearing silicate glass. Experiments with a CaF_2/granite ratio of 1:3 (ME-3b) show melt immiscibility with globules of fluorosilicate and oxysilicate glass, as well as minor rounded fluorite, which appears to represent residual unreacted starting material. An experiment without boron at this CaF_2/granite ratio (ME-30a) shows similar phase relations, but more unreacted fluorite. In the following, the bright melt in BSE images associated with high CaO and F contents will be referred to as fluorosilicate melt (*fm*) and the dark melt with lower CaO and F contents and higher SiO_2 as oxysilicate melt (*sm*). The run products and textures of the temperature series are described below and shown in Fig. 3.

3.1.1. a) 1200 °C experiments

The 1200 °C experiments (ME-14 and ME-8, Fig. 3A and B, respectively) represent the starting point for all P1 experiments. The run products show two liquids coexisting as spheroidal blebs or pools intensively mixed together. Fluorosilicate melt occurs both as large globules (*fm* dominant) with numerous small silicate spheroidal droplets (< 10 µm) inside, and as small droplets distributed in the silicate melt matrix (*sm* dominant). The *fm* dominant globules show a flow texture reflecting low viscosity of the immiscible liquids. No obvious gravitational segregation of either melt was observed at this temperature.

3.1.2. b) Slow cooling experiments

In the slow-cooling experiments, three phases can be observed: oxysilicate melt, fluorosilicate melt and fluorite. Fluorite minerals are dominantly present inside the fluorosilicate melt areas. At 1000 and 1100 °C the globule intermixing textures are identical to those at 1200 °C. The fluorosilicate melt is > 50% of the volume of the run product and has segregated to the bottom of the quartz capsule,

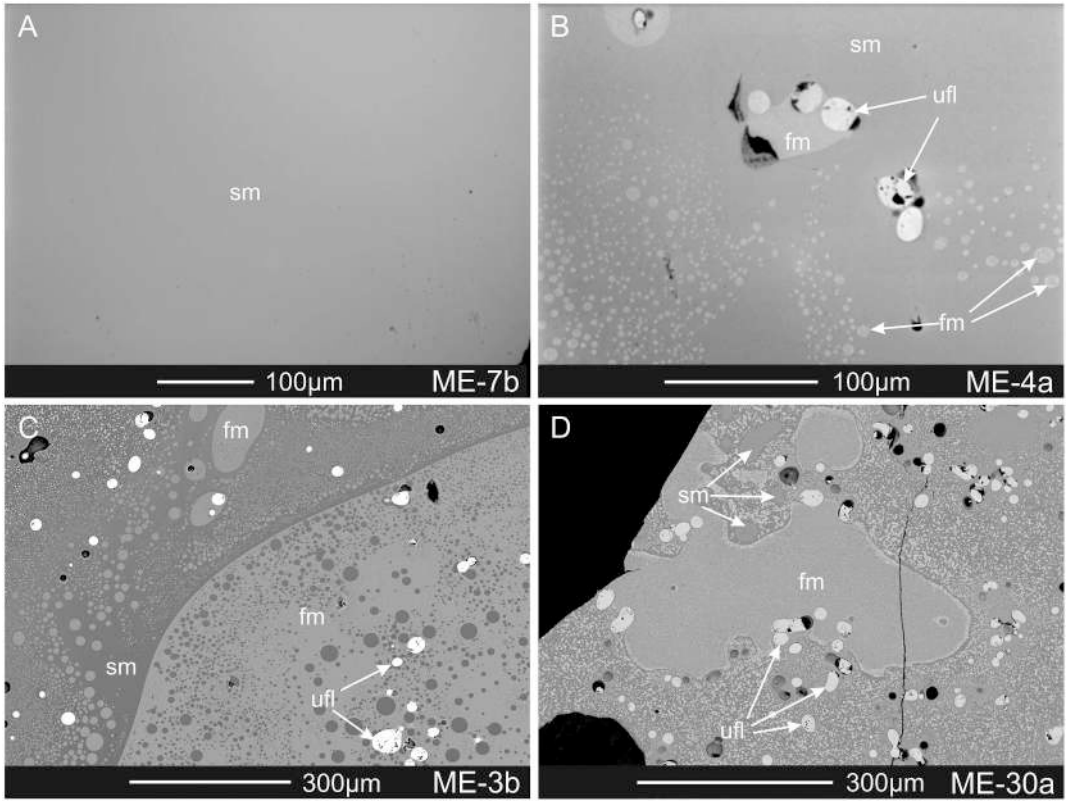

Fig. 2. Backscattered images of two typical exploratory experiments. (A) Experiment with low CaF2 starting composition (~2 wt% fluorine) resulting in a homogeneous silicate glass. (B) Local immiscibility of fluorosilicate and oxysiliscate liquids (sm and fm) at ~4 wt% F with some unreacted starting fluorite (ufl). (C, D) At high CaF_2 content (C: 6 wt% F, D: 10 wt% F), the experiment shows clear liquid immiscibility with fm and sm. There is a minor amount of unreacted fluorite.

indicating gravitational separation. The sizes of the rounded droplets range from a few microns to > 100 μm (Fig. 3C). At 900 °C and lower temperatures, oxysilicate spherical droplets are surrounded by aggregates of fluorite and wollastonite. The fluorite grains are usually < 3 μm in diameter with a spheroidal or liquid-like shape and occur in between wollastonite laths (Fig. 3E). Larger fluorite grains of 20 to 40 μm in diameter are also present (Fig. 3E) and their melt-fluorite contact textures indicate that these larger grains represent a

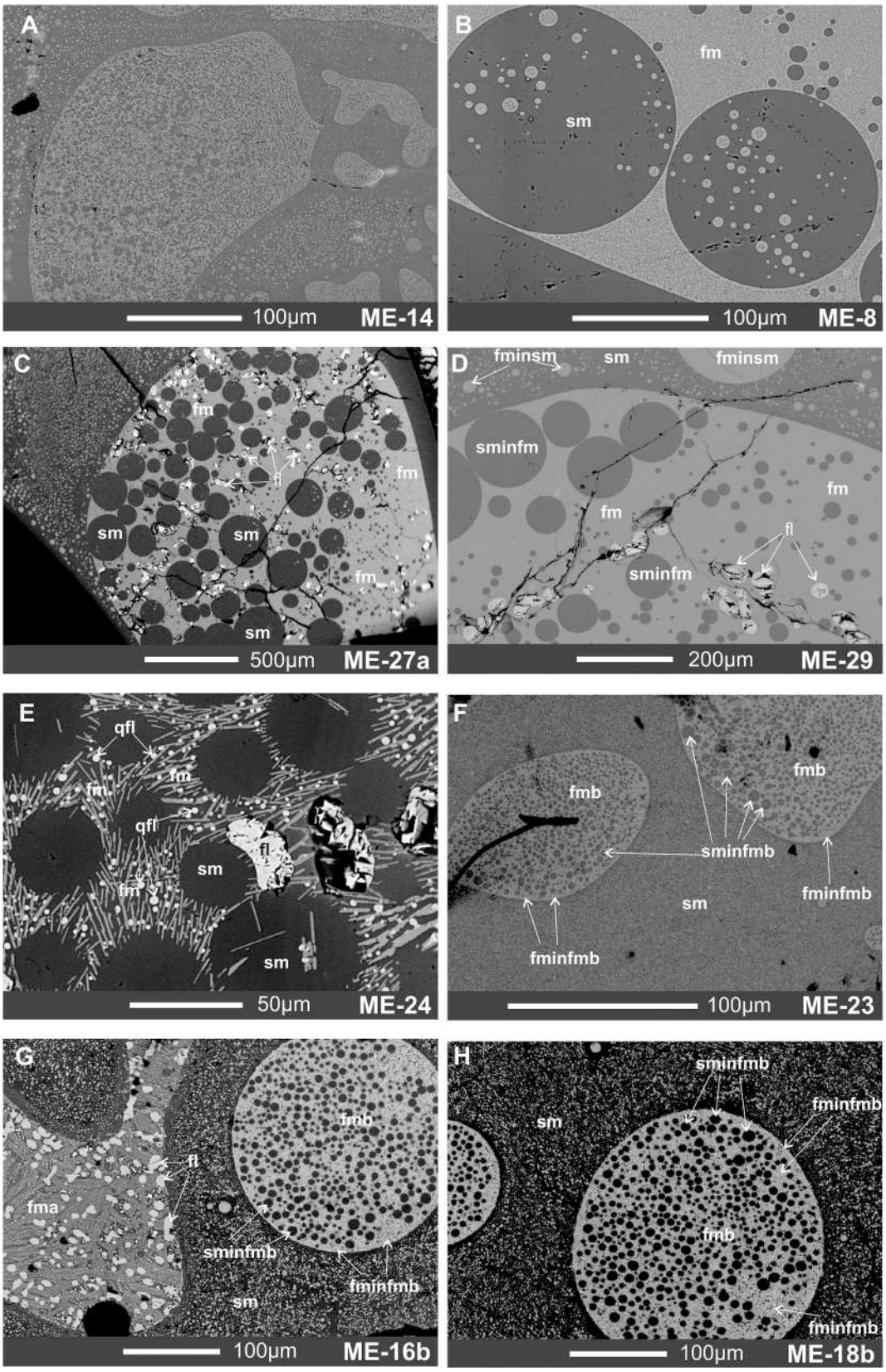

(caption on next page)

Fig. 3. Backscattered electron images of run products from P1 and P2 experiments at different temperatures. (A) After 5 h at 1200 °C (ME-14), the immiscible liquid globules are strongly mixed together but different domains can be identified: bright pools of fluorosilicate melt (fm) with numerous small dark droplets of silicate melt (sm) distributed inside and bright droplets of fm disseminated in the darker matrix of sm. (B) Better phase separation is observed at a 3-day run duration at 1200 °C (ME-8). (C) Slow cooling experiment at 1100 °C (ME-27a) showing good separation of immiscible liquids as well as fluorite crystallization. (D) Fast cooling experiment at 1100 °C (ME-29) showing identical textural characteristics to ME-27a. (E) Slow cooling experiment at 900 °C (ME-24) showing fluorosilicate melt quench into fluorite and wollastonite crystals. Note the size and shape difference between the coexisting fluorite crystals and the quench crystals. (F) Fast cooling experiment at 800 °C (ME-23) displaying the inherited textural characteristics of ME-14. (G) Fast cooling experiment at 700 °C (ME-16b) displaying a similar texture as ME-23 but with some of the fm-dominant globule crystalizing fluorite (fma). (H) ME-22 (slow cooling at 600 °C) showing no liquid immiscibility, with fluorite disseminated in homogeneous silicate melt.

solid phase that was present at run conditions. In contrast, we interpret the small fluorite crystals and the elongated wollastonite to represent quench crystals and for these domains to have been fluorosilicate melt at run conditions.

3.1.3. c) Fast cooling experiments

At 1000 and 1100 °C, the run products of the fast cooling experiments are identical to their slow cooling equivalents (Fig. 3D) with sharp separation of blebs of fluorosilicate and oxysilicate melt as well as showing fluorite crystallization. In contrast, experiments at ≤900 °C show a texture similar to that of ME-14 run at 1200 °C with globules of two immiscible melts, and lacking fluorite (Fig. 3F). The fluorosilicate melt domains (*fmb*, Fig. 3F) have segregated into dark oxysilicate melt globules in a bright fluorosilicate melt matrix, whereas the oxysilicate domains show the reverse with fluorite and wollastonite quench crystals (as determined by EDS). Fluorite crystallization is sometimes observed in the fluorosilicate melt domains (*fma*, Figs. 1G, H). These textures are not affected by duration at final temperature as evidenced by experiments ME-21b (280 h, 600 °C) and ME-13d (72 h, 600 °C).

3.2. Major element composition

The major compositions of the different phases in the experiments are summarized in Tables 4 and 5 and plotted in Fig. 4. Of the nine oxides analyzed by EMP, three (MgO, MnO and TiO_2) are < 0.5 wt% and are included in the trace element discussion. In all experiments, the silicate melt has a higher content of SiO_2, Al_2O_3, Na_2O and K_2O whereas the fluorosilicate melt has higher CaO and F. The FeO does not show a consistent preference for either melt and has similar concentrations in the two melts.

The 5-hour run at 1200 °C (ME-14) has the smallest compositional difference between the two immiscible liquids. In the slow cooling experiments, as temperature decreases, the major components in the silicate melt show a smooth and systematic change to increasing SiO_2 and Al_2O_3 content and decreasing CaO and F content. For the fluorosilicate melt, the CaO and F contents do not increase significantly as the temperature decreases nor is there a decrease in the SiO_2 and Al_2O_3 contents. The compositional gap between the two melts still widens (Fig. 4). The differences in Na_2O and K_2O contents between the two liquids also systematically increase, but no clear trend is present for FeO.

The major element compositions of both melts for the fast-cooling experiments at 1000 °C and 1100 °C are nearly identical to those in the equivalent slow-cooling experiments. From 900 to 700 °C, the major composition of the silicate melt (*sm-in-fmb*) is comparable to that of the silicate melt in the slow cooling experiments (*sm*) at the same temperatures. In contrast, the fluorosilicate melt (*fm-in-fmb*) is distinctly different in composition and appears to make a step-change to higher CaO and F content and lower SiO_2 and Al_2O_3 at 900 °C. Among lower temperature runs (800 °C to 500 °C), the changes in fluorosilicate melt composition become insignificant with only SiO_2 showing a small but consistent decrease. In both the slow- and fast-cooling runs, the miscibility gap is widest at the lowest temperature.

3.3. Experimental composition P2

Experiments with starting composition P2 show similar textures to those observed for the main P1 experimental series, but the fluorosilicate melt fraction is much smaller and mostly found as rinds on fluorite grains. Major element compositions of the oxysilicate melt are near identical to equivalent P1 experiments as are the systematic changes in composition with decreasing temperature. No liquid immiscibility was observed in experiment ME-22, which was run at 600 °C with a slow cooling rate (12 °C/h). Only oxysilicate melt and fluorite is present in the run product (Fig. 3H). There is no equivalent slow-cooling experiment in the P1 series, but the composition of the oxysilicate melt in ME-22 is close to that in the two 600 °C fast-cooling P1 experiments ME-21b and ME-13d (Fig. 6).

3.4. Element partitioning

The partitioning of elements between the immiscible melts is reported in this paper as the Nernst partition coefficient (D, e.g. $D_{La} = La_{fm}/La_{sm}$, concentrations in $^{mg}/_{kg}$) because of its simplicity and wide usage in experimental petrology. Partition coefficients for trace elements are summarized in Table 6 and shown in Fig. 5.

The alkali earth elements Mg, Ca, Sr, and Ba, the high field strength elements Ti, Zr, Hf, Nb, Ta, Th and U, and the REE preferentially partition into the fluorosilicate melt, whereas the alkali element (Na, K, Rb, Cs) and Al preferentially partition into the oxysilicate melt. This is consistent for all experiments and at all temperatures. Partition coefficients between the two melts are the highest for Ca, Mg and the REE, and the lowest for Rb and Cs. As temperature decreases, the partition coefficients become more extreme as the compositions of the two melts separate progressively, i.e. partition coefficients for the incompatible alkali elements decrease as temperature decreases whereas the D-values for the compatible REE and HFSE increase, although less pronounced for the HFSE. The Sc and Fe do not seem to be affected by the degree of the melt immiscibility or temperature, and have D-values close to unity, whereas Li, Pb and Zn have D-values above or close to unity at high temperatures but become incompatible in fluorosilicate melt as temperature decreases.

4. Discussion

4.1. The effect of boron on melt immiscibility

Boron was added to the experiments as a fluxing agent to lower the liquidus as well as the viscosity of the melts in our experiments. However, immiscibility in borosilicate systems is known (Veksler et al., 2002). To make sure that the immiscibility observed in our experiments was not the result of addition of B, we conducted one experiment without B at 1200 °C (ME-30a), which is equivalent to ME-14. The presence of fluorosilicate-oxysilicate immiscible melts in both ME-30a and ME-14 indicates that boron is not the cause of the melt immiscibility in the CaF_2-granite system. Moreover, boron does not show a preference for either melt (D-value ~ 1), suggesting that boron does not have an effect on the size of the miscibility gap either. ME-30a is fluorite-saturated whereas B-bearing experiments are super-liquidus at 1200 °C, showing that boron indeed lowers the liquidus of the system.

Table 4
Mean major element phase compositions (in wt%) of immiscible liquids in slow cooling experiments as analyzed by EMPA. The uncertainty on the data is given as 1 standard deviation in parenthesis.

Experiment	ME-8		ME-27a						ME-9c		ME-24		ME-15d		ME-32a	
Phase	sm	fm	sm	sm − in − sm	sm − in − fm	fm	fm − in − sm	fm − in − fm	sm	fm	sm	fm	sm	fm	sm	fm
Spot size (μm)	10,30,3	3,5	50	5	5	50	5	5	10	10	10	10	10	10	5	10
No. of Analyses	15	7	5	5	3	5	5	3	9	10	6	10	7	10	9	8
Na_2O	3.5 (1)	2.8(2)	3.9 (1)	3.9(2)	4.04(7)	3.04(5)	2.61(2)	2.93(6)	4.4 (1)	3.14(7)	5.1(2)	2.77(3)	4.9(8)	3.0(3)	5.1(2)	2.8(4)
K_2O	3.7(1)	2.3 (1)	4.23(9)	4.3 (1)	4.3(2)	1.7(1)	1.81(7)	1.84(4)	4.6 (1)	1.53(4)	4.4(2)	2.0(2)	5.0 (2)	2.41(2)	4.80(9)	2.0(2)
CaO	13.0(7)	25(1)	9.8(1)	9.6(5)	9(1)	27.3(6)	28.0 (4)	27.2(3)	7.7(2)	27.9(4)	2.97(3)	27(2)	1.5(4)	27(3)	1.3(1)	28(4)
MnO	0.14(9)	0.09(2)	0.06(2)	0.1(9)	0.2(1)	0.17(5)	0.15(9)	0.16(1)	0.12(9)	0.18(4)	0.07(1)	0.2(1)	0.2(2)	0.14(5)	0.11(3)	0.18(5)
MgO	0.03(1)	0.04(3)	0.02(3)	0.03(3)	0.02(1)	0.05(3)	0.04(2)	0.04(3)	0.03(3)	0.07(3)	0.05(4)	0.05(3)	0.07(5)	0.05(5)	0.06(3)	0.06(4)
TiO_2	0.19(2)	0.31(4)	0.18(4)	0.2(4)	0.21(5)	0.33(2)	0.37(4)	0.34(7)	0.17(6)	0.49(8)	0.29(4)	0.34(8)	0.31(7)	0.3(1)	0.29(8)	0.4(2)
FeO	3.04(9)	3.2 (1)	3.17(5)	3.3(1)	3.3(1)	3.76(5)	3.8(1)	3.7 (1)	3.3(8)	4.0(1)	4.1(3)	3.1(4)	4.6(4)	3.1(4)	4.5(1)	3.7(5)
Al_2O_3	9.08(1)	7.0(2)	10.19(5)	10.0 (1)	10(1)	6.6(1)	6.4(2)	6.47(6)	10.5 (1)	6.0(1)	11.1(1)	5.7(6)	11.4(2)	6.2(6)	11.6(2)	5.7(7)
SiO_2	64.0(9)	53.1(8)	65.7(4)	66.0 (8)	66(1)	50.7 (4)	49.7(6)	50.2(5)	66.8(7)	50.5(7)	68.6(6)	53(2)	69(1)	53(3)	70.6(9)	50(4)
F	4.4(4)	8.4(8)	2.6(3)	3.1 (3)	3.1 (4)	6.4(4)	8.9(3)	8.5(2)	2.0(3)	6.7(4)	0.75(2)	6(2)	0.6(3)	6.4(2)	0.4(2)	8(4)
Total (−O=2F)	99.79	98.27	98.72	99.26	99.08	97.41	98.04	97.76	98.89	97.52	97.11	98.08	96.82	98.73	98.58	98.33

4.2. Attainment of equilibrium

Attainment of equilibrium during the experiment is critical for the meaningful interpretation of resulting phase relations and D-values. In experiments run at or above 1000 °C, where droplets of difference sizes are readily available for analysis, the major and trace compositions of each melt are highly consistent with low compositional spread, and there is no statistically significant compositional difference between large and small droplets. This homogeneity is an important indicator for equilibrium in experiments (Watson, 1976). The gradual changes in major and trace element compositions in these experiments at various temperatures are systematic and consistent. Moreover, oxysilicate melt compositions are the same within error despite differences in cooling rate, run duration and starting composition even at low temperatures (e.g. ME-13d, ME-21b and ME-22 at 600 °C). Similarly, the slow- and fast-cooling experiments at 1100 °C (ME-27a and ME-29) are near-identical in textures, major element composition and D-values despite different cooling paths and run times. The same is true for experiments at 1000 °C (ME-9C and ME-40) in terms of major elements (fast-cooling run ME-40 was not analyzed for trace elements). Finally, and most importantly, the fluorosilicate melt inclusions in the silicate melt matrix (*fm-in-sm*, Fig. 3D) are the same composition as the large fluorosilicate melt globules (*fm*), and, vice versa, the silicate melt inclusions in the fluorosilicate melt globules (*sm-in-fm*) are the same composition as the silicate melt matrix (*sm*). These mutual inclusions represent an internal equilibrium check because the local bulk compositions of the fluorosilicate-dominant and oxysilicate-dominant domains are different so only at equilibrium will the liquid compositions be the same. We therefore conclude that the experiments represent equilibrium textures and compositions, although there are in part metastable extensions (see below).

4.3. Interpretation of textures: phase separation and globule growth

The interaction of the temperature and the cooling rate of the experiments predominantly control the phase separation as well as the growth mechanism of the liquid globules (Martin and Kushiro, 1991). A schematic illustration of the phase separation and globule growth in the experiments is shown in Fig. 7.

The starting texture of the experiments is represented by ME-14 and consists of irregularly shaped globules of fluorosilicate melt with numerous small droplets of silicate melt inside, and fluorosilicate melt droplets in the silicate melt matrix (Fig. 3A). This texture indicates that segregation of the two melts was incomplete. This is because, at high temperature, the small compositional contrasts promote the nucleation of immiscible liquid droplets (Veksler et al., 2010), and the segregation of the two liquids requires extensive periods of time (Charlier et al., 2013). Indeed, when run duration is extended to 3 days (ME-8) phase separation is more pronounced with bigger, more rounded and cleaner droplets of immiscible liquids (cf. Fig. 3A and B).

The original texture develops in different ways in the experiments at high and low temperature. At high temperature (1000 and 1100 °C), the size of the globules becomes larger, phase segregation improves, and no irregular globules as found in ME-14 persist (Fig. 3C, D). This indicates growth of globules, which is likely mainly accomplished by coalescence (Martin and Kushiro, 1991). This also shows that viscosity of the liquids at high temperature is low which allows them to move and merge. Cooling rate has no impact on textures at high temperature.

The textures develop in different ways for fast- and slow-cooling experiments at low temperatures. In the slow-cooling experiments, the low temperature runs (700 °C to 900 °C) exhibit similar textures to the high temperature runs with the exception that the fluorosilicate melt quenches to mineral aggregates. In the fast-cooling experiments, the low temperature runs (500 °C to 900 °C) inherit the starting texture and do not show significant growth or coalesce of globules, likely because of increased melt viscosity at low temperature. Instead, they show

Table 5
Mean major element phase compositions (in wt%) of immiscible liquids in the fast cooling experiments analyzed by EMPA. The uncertainty on the data is given as 1 standard deviation in parenthesis.

Experiment	ME-29		ME-40		ME-20		ME-23	
Spot size (μm)	10	10	5	10	3	3	5	10
No. of analyses	5	3	14	12	5	7	11	10
Phase	fm	sm	sm	fm	fm − in − fmb	sm − in − fmb	fm − infmb	sm − in − fmb
Na_2O	2.88(6)	3.97(5)	4.0(2)	3.01(8)	1.99(9)	4.7(2)	1.9(2)	5.13(9)
K_2O	1.9(1)	4.2(1)	4.2(1)	1.63(4)	1.51(8)	4.5(1)	1.6(2)	5.23(9)
CaO	27.5(7)	9.3(3)	9.1(4)	27.7(1)	43(1)	4.1(3)	43(3)	1.23(5)
MnO	0.3(2)	0.06(3)	0.07(2)	0.15(4)	0.14(2)	0.11(4)	0.18(7)	0.04(3)
MgO	0.03(2)	0.02(2)	0.05(2)	0.1(4)	0.01(2)	0.05(4)	0.02(2)	0.02(2)
TiO_2	0.35(3)	0.18(4)	0.22(4)	0.44(5)	0.17(6)	0.49(8)	0.25(9)	0.16(6)
FeO	3.8(1)	3.07(6)	3.21(6)	3.87(8)	2.0(1)	5.5(2)	2.7(7)	3.3(1)
Al_2O_3	6.6(2)	10.06(8)	10.6(1)	6.4(7)	3.9(2)	11.6(2)	3.8(5)	12.2(1)
SiO_2	50.5(9)	65.8(7)	65.0(8)	50.0(3)	38 (2)	65(1)	37.1(2)	71.2(7)
F	8.2(9)	3.3(3)	2.2(3)	6.4(3)	14(3)	1.2(3)	16(2)	0.3(3)
Total (−O=2F)	98.55	98.62	97.78	99.61	98.82	97.08	99.71	98.6

Experiment	ME-16b		ME-21b		ME-13d		ME-18b	
Spot size (μm)	5	5	5	5	10	10	5	5
No. of analyses	7	7	7	7	10	7	15	8
Phase	fm − in − fmb	sm − in − fmb	fm − in − fmb	sm − in − fmb	fm − in − fmb	sm − in − fmb	fm − in − fmb	sm − in − f-mb
Na_2O	1.7(1)	5.2(1)	2.0(3)	5.4(1)	1.9(2)	5.2(1)	2.0(2)	5.1(1)
K_2O	1.29(8)	5.34(4)	1.6(4)	5.4(7)	1.4(1)	5.03(7)	1.5(2)	5.2(1)
CaO	45(2)	0.83(7)	42(5)	0.58(3)	43(2)	1.2(2)	412(3)	1.2(1)
MnO	0.17(4)	0.1(1)	0.13(3)	0.07(9)	0.18(5)	0.07(6)	0.19(5)	0.05(4)
MgO	0.01(2)	0.02(2)	0.01(2)	0.03(2)	0.01(2)	0.04(2)	0.03(3)	0.01(2)
TiO_2	0.42(8)	0.1(4)	0.32(6)	0.12(5)	0.4(1)	0.12(3)	0.4(1)	0.12(4)
FeO	2.7(3)	3.39(8)	2.7(5)	3.36(9)	3.0(8)	3.25(6)	3.2(5)	3.4(1)
Al_2O_3	3.3(3)	12.9(1)	3.8(9)	12.5(2)	3.7(4)	12.1(1)	4(1)	11.8(1)
SiO_2	35(1)	72.0(7)	37(4)	71(1)	36(2)	71.7(4)	35(2)	70.6(3)
F	16(2)	0.4(2)	17(2)	0.2(2)	17(2)	0.2(2)	16(2)	0.3(2)
Total (−O=2F)	99.84	100.05	99.34	98.89	99.43	98.89	97.21	97.6

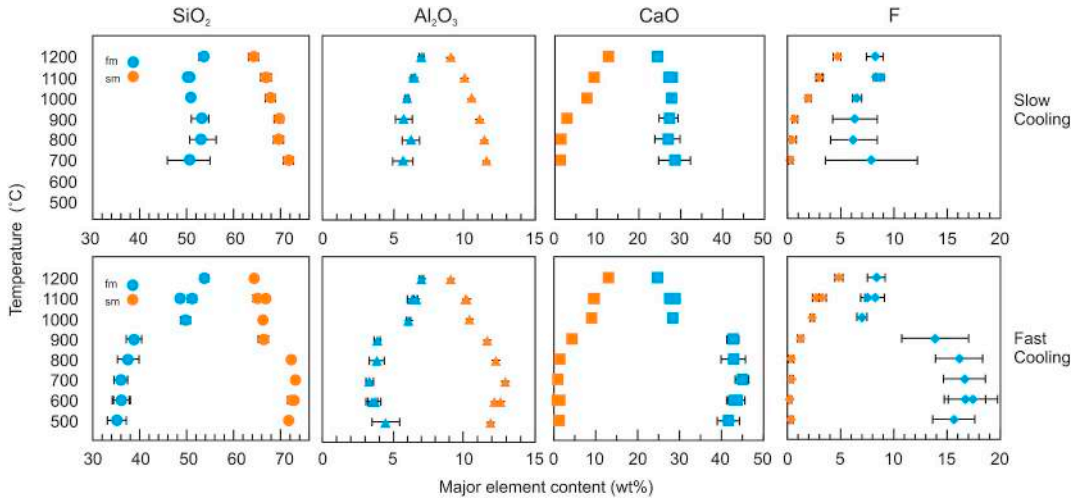

Fig. 4. Major element compositional differences between fluorosilicate (blue) and silicate (orange) melts in slow- and fast-cooling experiments from 1200 to 500 °C. Error bars represent the 1 standard deviation uncertainty on the mean. (For interpretation of the references to colour in this figure legend, the reader is referred to the web version of this article.)

compositional separation and re-equilibration within each globule, suggesting that this mainly takes place by diffusional exchange (see Martin and Kushiro, 1991). Despite the limited spatial reach of diffusion, global equilibrium is maintained as evidenced by the similarity in texture and the homogeneity in compositions for the phases throughout each experiment.

4.4. Major element compositions of the immiscible liquids

4.4.1. a) Slow cooling experiments

Compositionally, the F-rich immiscible component is a silicate melt with low SiO_2 content (~50 wt%) and high fluorine content (6–9 wt%). The F-poor component is an intermediate silicate melt at 1200 °C

Table 6
Partition coefficients calculated by mass of trace elements between the two immiscible liquids ($D^{fm}/_{sm}$). Uncertainties given in parenthesis are the 1 standard deviation on the mean. The symbol '/' stands for data not obtained because the deconvolution failed statistical tests (see Yang et al., 2018 for details).

Experiment	ME-8	ME-27a	ME-29	ME-9c	ME-20	ME-23	ME-16b	ME-13d	ME-21b	ME-18b
Li	1.6(1)	1.64(8)	1.85(9)	1.8(2)	0.6(3)	0.6(1)	0.34(9)	0.5(2)	0.47(8)	0.5(1)
B	1.24(8)	1.40(8)	1.52(5)	1.5(2)	0.07(5)	0.6(2)	0.3(1)	0.5(2)	0.57(2)	0.9(6)
Na	0.94(4)	0.76(3)	0.79(2)	0.71(5)	0.43(9)	0.36(5)	0.32(6)	0.4(1)	0.44(5)	0.47(9)
Mg	2.2(2)	3.3(3)	3.8(3)	3.9(3)	7(3)	12(5)	11(5)	8(4)	30(10)	40(20)
Si	0.89(3)	0.80(3)	0.82(1)	0.76(6)	0.46(6)	0.45(5)	0.44(6)	0.5(1)	0.45(5)	0.46(9)
K	0.65(3)	0.42(1)	0.41(2)	0.33(2)	0.19(5)	0.34(6)	0.17(4)	0.27(8)	0.33(4)	0.33(7)
Ca	2.1(1)	3.1(3)	3.5(3)	4.1(6)	10(1)	35(4)	54(7)	37(9)	72(7)	36(7)
Sc	0.92(8)	0.96(6)	1.0(1)	1.0(2)	/	/	/	/	/	/
Ti	1.42(8)	1.8(1)	2.0(1)	2.3(2)	2(1)	2.5(5)	2.4(9)	2.1(9)	2.4 (4)	2.8(7)
Mn	1.9(1)	2.5(2)	2.8(2)	3.2(3)	3.2(8)	5.6(1)	3.5(9)	3(1)	4.8(7)	6(1)
Fe	1.19(5)	1.26(5)	1.36(3)	1.33(8)	/	1.3(3)	0.8(5)	0.9(7)	/	1.1(4)
Zn	1.6(2)	1.8(2)	1.9(2)	2.2(3)	/	/	0.2(1)	0.5(4)	/	/
Ga	1.12(7)	0.97(5)	1.04(5)	1.0(1)	/	0.34(9)	0.08(9)	0.3(1)	0.22(8)	0.4(1)
Rb	0.57(3)	0.34(2)	0.32(2)	0.26(1)	0.09(4)	0.32(6)	0.14(5)	0.24(8)	0.25(4)	0.26(6)
Sr	1.8(1)	2.5(2)	2.8(2)	3.1(2)	4(1)	1.8(4)	2.5(7)	3(1)	4.3(8)	5(1)
Y	2.3(2)	3.4(3)	3.9(3)	4.5(5)	7(3)	18.1(6)	12(5)	13(8)	12(3)	18(5)
Zr	1.25(4)	1.43(7)	1.54(6)	1.63(8)	2.2(5)	1.7(3)	2.3(5)	1.7(5)	1.6(2)	1.8(4)
Nb	1.9(1)	2.5(2)	2.8(2)	3.3(3)	1.6(7)	3.1(6)	1.4(7)	2.0(7)	3.1(4)	3.3(7)
Cs	0.49(2)	0.27(2)	0.25(3)	0.19(2)	0.04(5)	0.11(4)	0.03(6)	0.14(7)	0.08(4)	0.12(4)
Ba	1.43(9)	1.8(1)	1.9(1)	2.0(2)	/	/	/	/	1.8(5)	2.0(6)
La	2.4(2)	3.7(4)	4.3(4)	5.1(6)	8(3)	13(4)	14(7)	10(7)	50(30)	40(20)
Ce	2.2(2)	3.5(3)	3.9(4)	4.7(5)	14(9)	13(4)	40(30)	20(10)	40(20)	30(10)
Pr	2.3(2)	3.6(4)	4.2(4)	5.0(6)	11(5)	18(6)	50(50)	20(10)	30(10)	60(40)
Nd	2.3(2)	3.5(3)	4.1(3)	4.8(5)	9(4)	21(8)	20(10)	13(7)	30(10)	40(20)
Sm	2.3(2)	3.5(3)	3.9(3)	4.8(4)	10(10)	19(8)	13(10)	8(5)	20(8)	30(20)
Eu	2.3(2)	3.5(4)	4.0(4)	4.8(6)	/	19(8)	8(5)	40(60)	40(30)	20(10)
Gd	2.3(2)	3.4(4)	4.1(3)	4.6(6)	/	40(40)	40(80)	40(70)	17(7)	20(10)
Dy	2.2(2)	3.3(3)	3.7(3)	4.4(4)	12(7)	20(10)	10(10)	12(8)	16(4)	30(10)
Ho	2.2(2)	3.2(3)	3.7(3)	4.3(5)	20(20)	18(8)	20(10)	11(7)	21(7)	20(10)
Tm	2.1(2)	3.1(3)	3.6(3)	4.0(5)	8(4)	16(7)	10(6)	7(4)	11(3)	20(10)
Yb	2.1(2)	3.1(3)	3.4(3)	4.0(3)	10(10)	12(4)	20(20)	8(5)	10(2)	16(7)
Lu	2.1(2)	3.0(3)	3.5(3)	3.9(4)	8(5)	13(5)	6(3)	6(4)	9(2)	15(7)
Hf	1.17(5)	1.34(6)	1.39(5)	1.54(7)	2.1(7)	1.6(4)	1.7(5)	1.4(6)	1.4(3)	1.5(4)
Ta	1.6(1)	2.0(1)	2.3(1)	2.6(2)	1.7(7)	2.7(5)	1.8(7)	1.9(7)	2.6(4)	2.7(6)
Pb	1.29(9)	1.2(6)	1.3(10)	1.3(9)	/	0.3(1)	/	0.3(1)	0.4(1)	0.6(2)
Th	1.8(1)	2.5(2)	2.8(2)	3.2(2)	4(1)	4.3(8)	6(2)	4(1)	5.2(8)	6(1)
U	1.5(1)	2.0(2)	2.3(2)	2.3(1)	3(1)	2.6(4)	2.9(8)	2.3(8)	3.1(5)	3.1(7)

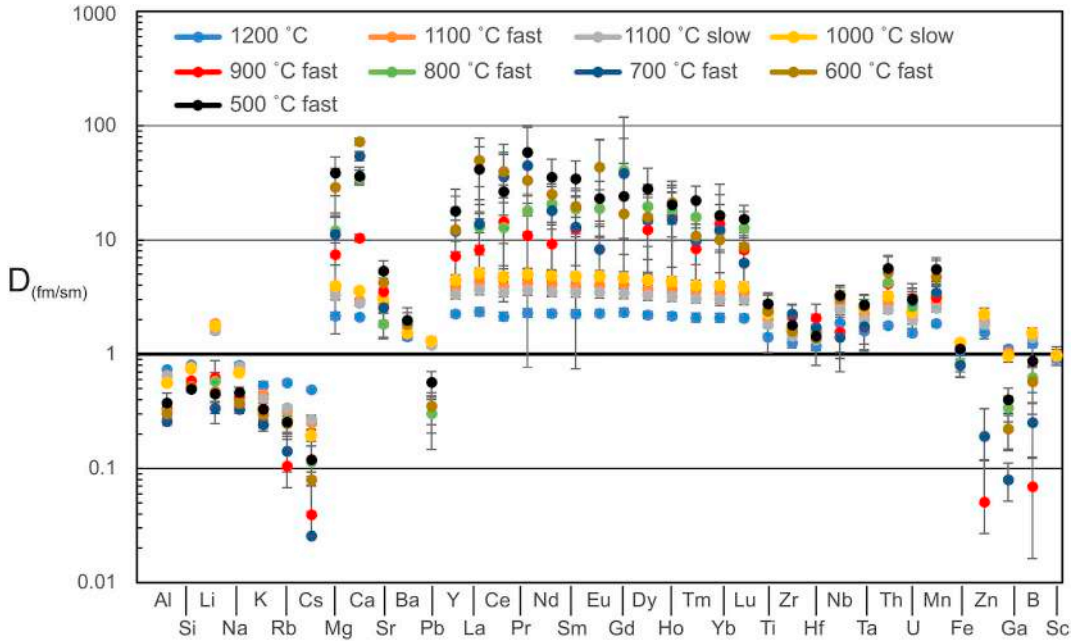

Fig. 5. Partition coefficients of trace element between the two immiscible liquids (D fm/sm) for temperatures from 1200 to 500 °C. The uncertainties shown are 1 standard deviation on the mean.

(~64 wt% SiO_2) evolving to a felsic silicate melt at lower temperatures (> 70 wt% SiO_2). Whereas the Ca and F contents significantly decrease in the silicate melt at lower temperatures, they do not increase in the accompanying fluorosilicate melt (Fig. 4). The fluorine content even decreases as temperature decreases although the large uncertainties for samples at low temperatures prohibit a conclusive assessment (Fig. 4). We attribute the constant Ca and F contents in the melt to being buffered by coexisting fluorite. The system reaches fluorite saturation between 1200 and 1100 °C. Fluorine concentrations in the oxysilicate melts at 800 °C to 1000 °C (0.6 to 2.0 wt%) are similar to those in the fluorite solubility experiments of Dolejš and Baker (2006) (0.8 to 1.7 wt %) at equivalent temperatures (800 °C to 950 °C), supporting that the fluorine concentration in our experiments are buffered by fluorite solubility. The slow-cooling experiment at 600 °C (ME-22, starting composition P2) displays a lack of liquid immiscibility, showing that between 700 °C and 600 °C, the immiscibility field reaches its lower boundary.

4.4.2. b) Fast cooling experiments

Compared to the slow-cooling experiments, the equivalent fast-cooling runs are characterized by the lack of fluorite and the appearance of *fmb* globules (Fig. 3F). This texture is observed in all fast-cooling runs at ≤900 °C and not seen in any of the slow-cooling runs. The bulk composition of the *fmb* globules is near-identical to that of the *fm* in the starting material (i.e. ME-14), but the globules have separated into a fluoride melt matrix (*fm-in-fmb*) enclosing silicate melt globules (*sm-in-fmb*). The compositional gap between these two immiscible liquids is bigger than in the equivalent slow-cooling experiments, mainly because of higher Ca and F content in *fm-in-fmb*. This is consistent with the lack of fluorite in these experiments. We interpret the texture and compositions to reflect a meta-stable state where fluorite nucleation has not taken place. This results in a larger miscibility gap as the fluorosilicate melt continues to shift to higher Ca and F contents with decreasing temperature, in contrast to the buffered composition in the slow-cooling experiments (Fig. 4). This behavior is contrary to the more typical scenario where fast cooling rates shrink the miscibility gap by providing insufficient time for complete phase separation (Martin and Kushiro, 1991). The silicate liquid in the slow- and fast-cooling runs from 900 to 700 °C is near-identical in composition indicating that it represents the equilibrium oxysilicate component of the miscibility gap (Fig. 4). The fast-cooling experiments therefore define the true shape of the fluorosilicate-oxysilicate miscibility gap, but the fluorosilicate limb is meta-stable below 900 °C.

The meta-stable state of the fluorosilicate globules in these fast-cooling experiments is further confirmed by their conversion to a stable assemblage (*fma*) of fluorite, silicate melt and wollastonite in some experiments (ME-16b, ME-13d, ME-18b). Both the stable and meta-stable states are observed in these experiments (Fig. 3G) and the conversion was likely triggered by local fluorite nucleation. However, the two runs at 600 °C with different run duration (72 h vs. 280 h) both contain the meta-stable fluorosilicate immiscible liquid with similar major element composition, indicating that these metastable liquids can potentially be stable for long periods of time if not disturbed.

4.4.3. c) Phase relations in the CaF_2-granite system

The phase diagram constructed from the experiments is shown in Fig. 6. The system is above liquidus at 1200 °C with two immiscible liquids and reaches fluorite saturation between 1200 and 1100 °C. Under slow-cooling conditions, the three phases oxysilicate melt, fluorosilicate melt and fluorite persist down to 700 °C. Because of crystallization of fluorite, the Ca and F contents in both liquids decrease. The miscibility gap reaches its lower boundary between 700 and 600 °C in a peritectic reaction where the fluorosilicate melt reacts to fluorite and oxysilicate melt (Fig. 6B). Under rapid cooling condition, the undercooling prohibits the nucleation of fluorite and produces a metastable fluorosilicate liquid that has significantly higher Ca and F contents than in its slow-cooled counterpart, resulting in a wider miscibility gap below 1000 °C (Fig. 6A). This metastable fluorosilicate liquid persists down to at least 500 °C.

4.5. Trace element partitioning between the immiscible melts

There is strong fractionation of the trace elements between the fluorosilicate and oxysilicate melts (Fig. 5), with the HFSE and REE strongly partitioning into the fluorosilicate melt, whereas the alkalis prefer the silicate melt. This behavior is consistent among all experiments and is governed by differences in the melt structure. It has been shown in previous studies (Hess, 1995; Hudon and Baker, 2002; Veksler

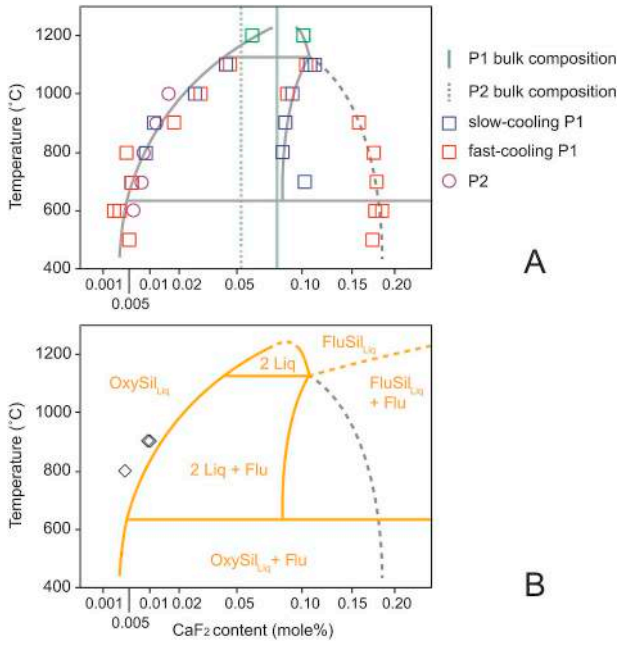

Fig. 6. Phase diagram for the CaF2-granite system constructed from the experiments. A shows the compositions of all experiments, with B showing the phase assemblages for each field. The grey dashed line represents the metastable extension of the miscibility gap, whereas the yellow dashed lines are inferred. The grey diamonds are data from natural immiscible silicate liquid from Vasyukova and Williams-Jones (2014). The x-axis is non-linear to illustrate the compositional evolution of the silicate liquid. (For interpretation of the references to colour in this figure legend, the reader is referred to the web version of this article.)

et al., 2005) that element partitioning between ionic (salt) and covalent (silicate) immiscible liquids is primarily governed by the ionic potential of the elements, as defined by the formal charge (Z) over the ionic radius (r). Although the two immiscible melts in this study are both silicate melts, the fluorosilicate melt will have a stronger ionic character than the oxysilicate melt. To evaluate the ionic potential dependence for the CaF_2-granite system, the partition coefficients for two experiments at 1100 and 500 °C, respectively, are plotted against Z/r (Fig. 8). The two temperatures display the same pattern, despite the more than one order of magnitude difference in the D-values for several of the elements. These plots share a striking similarity with the partitioning pattern for Ca-Mg-fluoride – silicate immiscible melts (Veksler et al., 2005), borosilicate immiscible liquids (Veksler et al., 2006) and Ca-carbonatite – silicate immiscible melts (Martin et al., 2013). Similar patterns are also observed in other molten salt-silicate systems (Veksler et al., 2012), gabbroic-granitic immiscible melts (Schmidt et al., 2006), and are also in good agreement with the relationships between partitioning and Z/r for simple oxide-silica binaries (Hess and Rutherford, 1974; Hudon and Baker, 2002; Ryerson and Hess, 1978). This consistency in the D vs. Z/r behaviour suggests that interpolation to obtain D-values based on Z/r for elements not determined experimentally is warranted.

According to (Schmidt et al., 2006), the elements can be grouped into three categories based on their partitioning behavior and oxygen bonding environment: (1) network formers with oxygen coordination numbers ≤4 (Si, Al, Ga, Pb, B). These elements partition into the silicate melt as they make up (e.g. Si and Al) or substitute for (e.g. Ga) the major elements in the melt polymers. (2) The alkalis and alkali earths, whose partitioning behavior is defined by a strong dependence on the ionic potential (Z/r). As the ionic potential increases, the preference for the ionic melt increases steeply and, hence, $D_{Cs} < D_{Rb} < D_K < D_{Na} < D_{Li} < D_{Ba} < D_{Sr} < D_{Ca} \leq D_{Mg}$. These elements are network modifiers and the stronger the element-oxygen bond, the stronger the tendency to change the melt structure and hence instigate immiscibility (Hudon and Baker, 2002). (3) The rare earth and high field strength elements. These elements are non-bridging-oxygen coordinated in silicate melt (Ellison and Hess, 1990). The REE partition strongly into fluorosilicate melt, because not only are non-bridging oxygens not readily available in the highly polymerized silicate melt phase, but the REE also form strong complexes with fluorine (Ponader and Brown, 1989), which is more abundant in the fluorosilicate melt. As the atomic number increases, the partition coefficients for the REE decrease, as the REE are increasingly amphoteric at higher atomic numbers (Hudon and Baker, 2002; Veksler et al., 2006). The HFSE (Ti, Zr, Hf, Nb, Ta, Th, U) partition into fluoride melt with D values lower than the REE, which is explained by these elements having lower coordination numbers (4–6) than the REE (6–8) (Schmidt et al., 2006) and do not exhibit as great an affinity to fluorine as the REE.

4.5.1. Effect of temperature and miscibility gap width on element partitioning

The solution model in Schmidt et al. (2006) predicts that the trace element partition coefficients are dependent on the size of the miscibility gap, which is consistent with our experiments, as well as those reported by Martin et al. (2013), Veksler et al. (2006) and Watson (1976). The size of the miscibility gap is directly controlled by temperature in our experiments and the effects of temperature and miscibility gap width on partitioning are therefore discussed together here.

The miscibility gap narrows with increasing temperature and the melts therefore become more similar, which should result in the partition coefficients converging towards unity (Martin et al., 2013). Indeed, D values show the largest contrast (i.e. the highest and lowest values) at low temperatures and for the widest miscibility gap (Fig. 5). The systematic differences between the three groups of elements, and the trends within each group are maintained, but become more pronounced for the wider miscibility gaps (Fig. 8). This results in marked changes in element ratios (e.g. Ca/Pb, LREE/HREE). As a result, low temperature immiscibility can significantly fractionate the LREE from the HREE. The stronger contrast in D values at lower temperatures shows that the immiscible melts become more selective in trace elements as temperature decreases, which is also consistent with a more rigid structure for the polymerized silicate melt at lower temperatures.

4.6. Geological implication of ca fluoride-silicate melt immiscibility

Our experiments confirm the presence of a miscibility gap in the CaF_2-granite system over a wide range of temperatures, and thereby support the interpretation of coexisting F-rich and F-poor silicate melt inclusions as immiscible liquids in natural systems (e.g. Vasyukova and Williams-Jones, 2014). Fluorine contents in natural igneous rocks are on average 0.07 wt% in basalt and 0.2 wt% in evolved rocks (GEOROC database), although higher concentrations have been found. Comprehensive studies by Dolejš and Baker (2007a, 2007b) and Dolejš and Zajacz (2018) report that fluorine content in natural silicic suites can be as high as 3.9 wt%, and extreme F-contents up to 6 wt% have been found in rare topazite dikes (e.g., Kortemeier and Burt, 1988). Experiments on CaF_2 – haplogranite systems give a F-content in the melt of 1.7 wt% at 950 °C and 100 MPa at fluorite saturation with Ca in excess where melt F-content is controlled by the solubility of fluorite (Dolejš and Baker, 2006). From our experiments, melt immiscibility will be encountered when the bulk F-content exceeds that which can be accommodated by the silicate melt, which is approximately 0.5 wt% below 800 °C, and then rapidly increases with temperature to > 4.4 wt % at 1200 °C (Fig. 4). At low temperatures, F-concentrations in natural igneous rocks therefore extend into the immiscibility field. The melt inclusions found in Vasyukova and Williams-Jones (2014) are associated with temperatures of 900 to 950 °C, and our experiments suggest these would saturate an immiscible liquid at approximately 0.75–1.2 wt % F which is similar to the F content of the silicate glass (1.04–1.67 wt

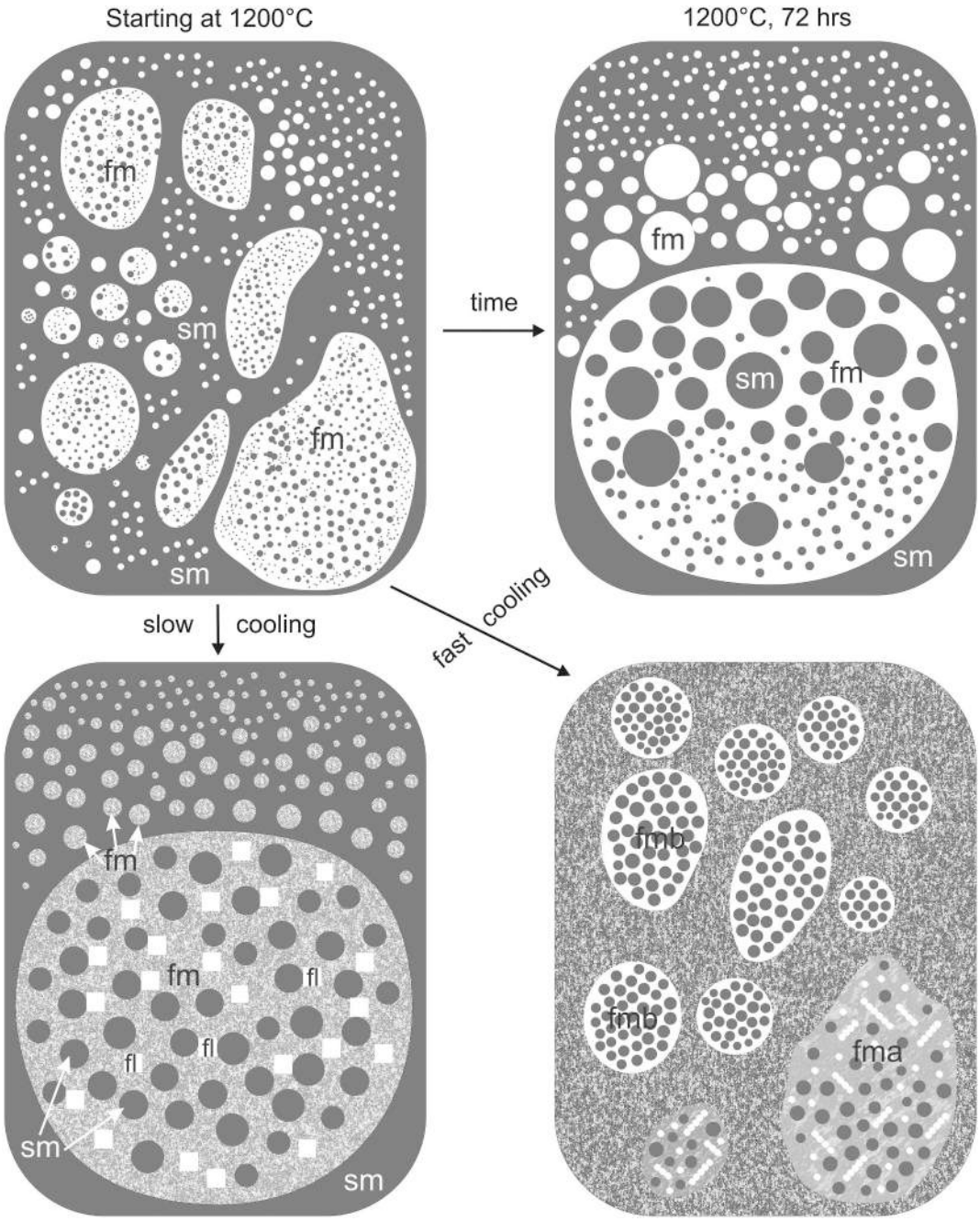

Fig. 7. Schematic illustration of the effect of temperature and cooling rate on mineralogy and textures of the run products.

%) (Figs. 4, 6) that is in contact with F-rich glass in the melt inclusions (Type 2 melt inclusion in Vasyukova and Williams-Jones, 2014), indicating good agreement between experimental results and natural observations.

The granite-CaF_2 phase diagram derived from our experiments (Fig. 6B) suggests that liquid immiscibility is reached before fluorite saturation. This indicates that calcic magmas would be able to evolve to the liquid immiscibility domain by residual enrichment of F given the incompatibility of F in the main fractionating minerals (e.g. olivine, pyroxene, plagioclase, sanidine, quartz). However, reports of fluorosilicate melts in natural samples are very rare. This will mainly be the result of the required high F contents being rare in nature (Dolejš and Baker, 2007a, 2007b), but missed observations and misidentification cannot be ruled out. Indeed, the fluorosilicate immiscible melt is nearly unquenchable even when drop-quenched as in our experiments and crystallizes to fluorite and silicates. Moreover, larger magmatic bodies, including plutons, cool slowly and can be expected to lose evidence for liquid immiscibility when the system reaches the fluorosilicate terminal peritectic reaction around 600 °C. Below this temperature fluorite hosts the F that was originally present in the immiscible melt. Fluorite is the most common F-phase in evolved F-rich magmatic rocks and our results suggest that at least some of this may represent original immiscible fluorosilicate liquid. Even though clear textural evidence is rarely available, our results show that aggregates of fluorite in these systems are likely a result of crystallization of an immiscible fluorosilicate liquid. Rapid cooling from high to low temperature would result in better preservation potential for immiscible fluorosilicate liquid, which is consistent with the clearest natural examples that have been reported so far: the quenched lava in the Oldoinyo Lengai 1993 eruption (Potter et al., 2017) and the melt pocket with chilled margin described in

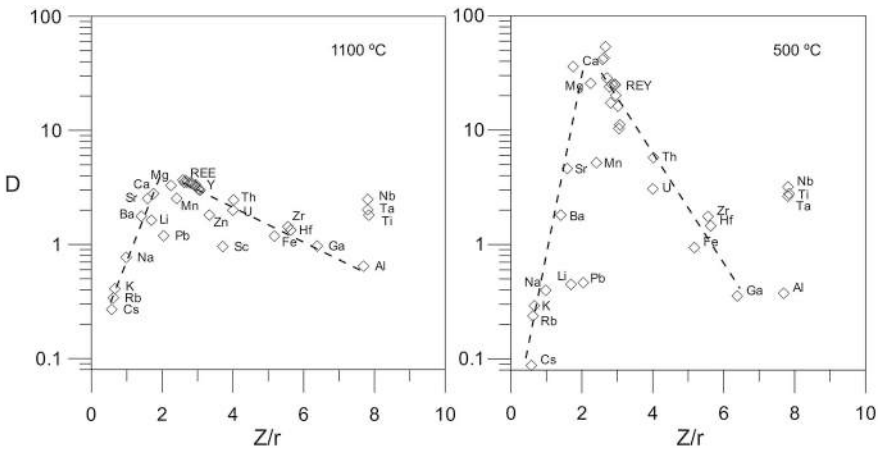

Fig. 8. Logarithms of the two-liquid trace element partition coefficients (D fm/sm) plotted against ionic potentials (Z/r) in experiments at 1100 °C and 500 °C. The ionic radii are taken from (Shannon, 1976), The charge of the elements is assumed to be the highest oxidation state given that our experiments were conducted in air. The coordination number chosen for each element is based on (Hudon and Baker, 2002; Schmidt et al., 2006; Veksler et al., 2006; Martin et al., 2013).

Vasyukova and Williams-Jones (2016), both of which are associated with rapid cooling.

The occurrence of F-induced liquid immiscibility has important implications given the strong fractionation of trace elements between the two melts, especially at the lower temperatures relevant to granite magmatism. The REE, in particular, are strongly enriched in the fluorosilicate melt. The higher density of this melt allows it to segregate, aided by its low viscosity, as observed in our experiments. The fluorosilicate melt would therefore not only sequester the REE, but fractionate them from the host silicate melt, which has been suggested as a potential mineralizing process (Vasyukova and Williams-Jones, 2014, 2016).

5. Conclusion

This study experimentally confirms the presence of liquid immiscibility in the CaF_2-granite system and maps out the miscibility gap from 500 to 1200 °C at ambient pressure. The miscibility gap is encountered at ~0.5 wt% F at low temperature and then rapidly increases at higher temperatures (0.75 wt% at 900 °C, 3.1 wt% at 1100 °C and 4.4 wt% at 1200 °C). Cooling rate has an important impact on the miscibility gap. Fast cooling results in metastable extension of the fluorosilicate limb of the miscibility gap by inhibiting fluorite crystallization, and extends the immiscibility field down to at least 500 °C. At slow cooling rates, fluorite is present, and the fluorosilicate melt is buffered in composition by fluorite resulting in a much-reduced miscibility gap. The system reaches a peritectic reaction between 600 °C and 700 °C that converts the fluorosilicate melt to fluorite and oxysilicate melt, which represent the terminal stability of liquid immiscibility.

Partition coefficients for trace elements between these fluorosilicate and oxysilicate immiscible melts show that the alkali earths, high field strength elements and especially the rare earth elements strongly partition into the fluorosilicate liquid, whereas the alkalis, amphoteric and network-forming elements partition into the oxysilicate liquid. Partitioning systematics are primarily controlled by the ionic potential and the bonding environment of the trace elements and further depend on the width of the miscibility gap which is in turn controlled by temperature. Partition coefficients move away from unity as the miscibility gap widens and the D values for rare earth elements increase over an order of magnitude from high temperature to low temperature. The strong preference of the fluorosilicate melt for the REE makes F-induced liquid immiscibility a magmatic REE concentration mechanism, whereas its higher density compared to the coexisting oxysilicate melt provides for a potential fractionation mechanism. Combined, this suggests that liquid immiscibility could act as an ore forming mechanism in magmatic REE deposits.

Declarations of interest

None.

Acknowledgements

This study was funded through a China Scholarship Council scholarship and Diversification de l'Exploration Minérale au Québec (DIVEX) grant to LY, and Robert Wares research stipend, Canadian Foundation for Innovation (CFI) Leaders Opportunity Fund grant and Natural Sciences and Engineering Research Council (NSERC) Discovery grant to VJvH. We are grateful to Olga Vasyukova and Anthony E. Williams-Jones for helpful discussions and providing the starting granite for the experiments, Iain Samson for valuable suggestions, and Lang Shi and Anna Jung for helping with the chemical analyses.

References

Andreeva, I.A., Kovalenko, V.I., Yarmolyuk, V.V., Listratova, E.N., Kononkova, N.N., 2007. Immiscibility of silicate and salt (Li, Na, F) melts in comendite at the Zaart Khudag ore occurrence, Central Mongolia: evidence from melt inclusions. Dokl. Earth Sci. 414, 655–660. https://doi.org/10.1134/S1028334X07040368.

Berezhnoi, A.S., 1951. Some data on the system MgO-CaF_2-SiO_2 and their signifi cance in the technology of refractory materials. Dopovidi Akademii Nauk Ukrainskoi RSR 248–252.

Charlier, B., Namur, O., Grove, T.L., 2013. Compositional and kinetic controls on liquid immiscibility in ferrobasalt–rhyolite volcanic and plutonic series. Geochim. Cosmochim. Acta 113, 79–93. https://doi.org/10.1016/j.gca.2013.03.017.

Chorlton, L.B., Martin, E.F., 1978. The effect of boron on the granite solidus. Can. Mineral. 16, 239–244.

Dawson, J.B., Pinkerton, H., Norton, G.E., Pyle, D.M., Browning, P., Jackson, D., Fallick, A.E., 1995. Petrology and Geochemistry of Oldoinyo Lengai Lavas Extruded in November 1988: Magma Source, Ascent and Crystallization. In: Carbonatite Volcanism. IAVCEI Proceedings in Volcanology Springer, Berlin, Heidelberg, pp. 47–69. https://doi.org/10.1007/978-3-642-79182-6_5.

Dingwell, D.B., Knoche, R., Webb, S.L., Pichavant, M., 1992. The effect of B_2O_3 on the viscosity of haplogranitic liquids. Am. Mineral. 457–461.

Dolejš, D., 2005. Evidence for fluoride melts in Earth's mantle formed by liquid immiscibility: comment and reply comment. Geology 33https://doi.org/10.1130/0091-7613-33.1.e76. e76–e76.

Dolejš, D., Baker, D.R., 2006. Fluorite solubility in hydrous haplogranitic melts at 100 MPa. Chem. Geol. 225, 40–60.

Dolejš, D., Baker, D.R., 2007a. Liquidus equilibria in the System K_2O-Na_2O-Al_2O_3-SiO_2-F_2O_1-H_2O to 100 MPa: I. Silicate-fluoride liquid immiscibility in anhydrous systems. J. Petrol. 48, 785–806. https://doi.org/10.1093/petrology/egm001.

Dolejš, D., Baker, D.R., 2007b. Liquidus Equilibria in the System K_2O-Na_2O-Al_2O_3-SiO_2-F_2O_1-H_2O to 100 MPa: II. Differentiation paths of fluorosilicic magmas in hydrous systems. J. Petrol. 48, 807–828. https://doi.org/10.1093/petrology/egm002.

Dolejš, D., Zajacz, Z., 2018. Halogens in silicic magmas and their hydrothermal systems. In: Harlov, D.E., Aranovich, L. (Eds.), The Role of Halogens in Terrestrial and Extraterrestrial Geochemical Processes: Surface, Crust, and Mantle. Springer Geochemistry. Springer International Publishing, Cham, pp. 431–543. https://doi.org/10.1007/978-3-319-61667-4_7.

Ellison, A.J.G., Hess, P.C., 1990. Lanthanides in silicate glasses: a vibrational spectroscopic study. J. Geophys. Res. 95, 15717. https://doi.org/10.1029/JB095iB10p15717.

Fleet, M.E., Stone, W.E., Crocket, J.H., 1991. Partitioning of palladium, iridium, and

platinum between sulfide liquid and basalt melt: effects of melt composition, concentration, and oxygen fugacity. Geochim. Cosmochim. Acta 55, 2545–2554. https://doi.org/10.1016/0016-7037(91)90372-C.
Gramenitskiy, Y.N., Shchekina, T.I., 1994. Phase relationships in the liquidus part of a granitic system containing fluorine. Geochem. Int. 52–70.
Hellstrom, J., Paton, C., Woodhead, J., Hergt, J., 2008. Iolite: software for spatially resolved LA-(quad and MC) ICPMS analysis. Mineralogical Association of Canada Short Course Series 40, 343–348.
Hess, P.C., 1995. Thermodynamic mixing properties and the structure of silicate melts. Rev. Mineral. Geochem. 32, 147–189.
Hess, P.C., Rutherford, M.J., 1974. Element fractionation between immiscible melts. In: Lunar and Planetary Science Conference.
Hillert, L., 1964. The phase diagram SiO_2-CaF_2. Acta Chem. Scand. 18, 2411. https://doi.org/10.3891/acta.chem.scand.18-2411.
Hudon, P., Baker, D.R., 2002. The nature of phase separation in binary oxide melts and glasses. I. Silicate systems. J. Non-Cryst. Solids 303, 299–345. https://doi.org/10.1016/S0022-3093(02)01043-8.
Jochum, K.P., Stoll, B., 2008. Reference materials for elemental and isotopic analyses by LA-(MC)-ICP-MS: successes and outstanding needs. Laser Ablation ICP-MS in the Earth Sciences: Current Practices and Outstanding Issues 40, 147–168.
Jung, I.H., Van Ende, M.-A., Kim, D.-G., Konar, B., Kwon, S.-Y., 2015. Thermodynamic database for oxy-fluoride mold flux, CaO-MgO-Na_2O-K_2O-Li_2O-Al_2O_3-SiO_2-ZrO_2-F. Asia Steel 476–477.
Kamenetsky, V.S., Naumov, V.B., Davidson, P., van Achterbergh, E., Ryan, C.G., 2004. Immiscibility between silicate magmas and aqueous fluids: a melt inclusion pursuit into the magmatic-hydrothermal transition in the Omsukchan Granite (NE Russia). Chemical Geology, The Magmatic to Hydrothermal Transition and Its Bearing on Ore-forming Processes 210, 73–90. https://doi.org/10.1016/j.chemgeo.2004.06.016.
Klemme, S., 2004. Evidence for fluoride melts in Earth's mantle formed by liquid immiscibility. Geology 32, 441–444. https://doi.org/10.1130/G20328.1.
Klemme, S., 2005. Evidence for fluoride melts in Earth's mantle formed by liquid immiscibility: comment and reply REPLY. Geology 33https://doi.org/10.1130/0091-7613-33.1.e77. e77–e77.
Kogarko, L.N., Krigman, L.D., 1970. Phase equilibria in the system nepheline-NaF. Geokhimiya 2, 162–168.
Kortemeier, W.T.B., Burt, D.M., 1988. Ongonite and topazite dikes in the Flying W ranch area, Tonto basin, Arizona. Am. Mineral. 507–523.
Longerich, H.P., Jackson, S.E., Günther, D., 1996. Inter-laboratory note. Laser ablation inductively coupled plasma mass spectrometric transient signal data acquisition and analyte concentration calculation. J. Anal. At. Spectrom. 11, 899–904. https://doi.org/10.1039/JA9961100899.
Martin, B., Kushiro, I., 1991. Immiscibility synthesis as an indication of cooling rates of basalts. J. Volcanol. Geotherm. Res. 45, 289–310. https://doi.org/10.1016/0377-0273(91)90064-7.
Martin, L.H.J., Schmidt, M.W., Mattsson, H.B., Guenther, D., 2013. Element partitioning between immiscible carbonatite and silicate melts for dry and H_2O-bearing Systems at 1–3 GPa. J. Petrol. 54, 2301–2338. https://doi.org/10.1093/petrology/egt048.
Peach, C.L., Mathez, E.A., Keays, R.R., Reeves, S.J., 1994. Experimentally determined sulfide melt-silicate melt partition coefficients for iridium and palladium. Chemical Geology, Trace-element Partitioning with Application to Magmatic Processes 117, 361–377. https://doi.org/10.1016/0009-2541(94)90138-4.
Peretyazhko, I.S., Zagorsky, V.Y., Tsareva, E.A., Sapozhnikov, A.N., 2007. Immiscibility of calcium fluoride and aluminosilicate melts in ongonite from the Ary-Bulak intrusion, Eastern Transbaikal region. Dokl. Earth Sci. 413, 315–320. https://doi.org/10.1134/S1028334X07020419.
Ponader, C.W., Brown, G.E., 1989. Rare earth elements in silicate glassmelt systems: II. Interactions of La, Gd, and Yb with halogens. Geochim. Cosmochim. Acta 53, 2905–2914. https://doi.org/10.1016/0016-7037(89)90167-1.
Potter, N.J., Kamenetsky, V.S., Simonetti, A., Goemann, K., 2017. Different types of liquid immiscibility in carbonatite magmas: a case study of the Oldoinyo Lengai 1993 lava and melt inclusions. Chemical Geology, The Role of Intraplate Magmas and Their Inclusions in Earth's Mantle Evolution 455, 376–384. https://doi.org/10.1016/j.chemgeo.2016.09.034.
Roedder, E., 1992. Fluid inclusion evidence for immiscibility in magmatic differentiation. Geochim. Cosmochim. Acta 56, 5–20.
Ryerson, F.J., Hess, P.C., 1978. Experimental trace element geochemistry implications of liquid-liquid distribution coefficients to mineral-liquid partitioning. Geochim. Cosmochim. Acta 42, 921–932. https://doi.org/10.1016/0016-7037(78)90103-5.
Schmidt, M.W., Connolly, J.a.D., Günther, D., Bogaerts, M., 2006. Element partitioning: the role of melt structure and composition. Science 312, 1646–1650. https://doi.org/10.1126/science.1126690.
Shannon, R.D., 1976. Revised effective ionic radii and systematic studies of interatomic distances in halides and chalcogenides. Acta Crystallogr. Sect. A 32, 751–767. https://doi.org/10.1107/S0567739476001551.
Solovova, I.P., Girnis, A.V., Kovalenko, V.I., 2010. Fluoride and chloride melts included in phenocrysts of agpaitic acid volcanic rocks from Pantelleria Island. Dokl. Earth Sci. 433, 978–981. https://doi.org/10.1134/S1028334X10070287.
Stix, J., Gauthier, G., Ludden, J.N., 1995. A critical look at quantitative laser ablation ICP-MS analysis of natural and synthetic glasses. Can. Mineral. 33, 435–444.
Ueda, S., Maeda, M., 1999. Phase-diagram study for the Al_2O_3-CaF_2-SiO_2 system. Metall. Mater. Trans. B 30, 921–925. https://doi.org/10.1007/s11663-999-0097-3.
Vasyukova, O., Williams-Jones, A.E., 2014. Fluoride–silicate melt immiscibility and its role in REE ore formation: evidence from the Strange Lake rare metal deposit, Québec-Labrador, Canada. Geochim. Cosmochim. Acta 139, 110–130. https://doi.org/10.1016/j.gca.2014.04.031.
Vasyukova, O., Williams-Jones, A.E., 2016. The evolution of immiscible silicate and fluoride melts: Implications for REE ore-genesis. Geochim. Cosmochim. Acta 172, 205–224. https://doi.org/10.1016/j.gca.2015.09.018.
Veksler, I.V., 2004. Liquid immiscibility and its role at the magmatic–hydrothermal transition: a summary of experimental studies. Chemical Geology, The Magmatic to Hydrothermal Transition and its Bearing on Ore-forming Processes 210, 7–31. https://doi.org/10.1016/j.chemgeo.2004.06.002.
Veksler, I.V., Dorfman, A.M., Danyushevsky, L.V., Jakobsen, J.K., Dingwell, D.B., 2006. Immiscible silicate liquid partition coefficients: implications for crystal-melt element partitioning and basalt petrogenesis. Contrib. Mineral. Petrol. 152, 685–702. https://doi.org/10.1007/s00410-006-0127-y.
Veksler, I.V., Dorfman, A.M., Dingwell, D.B., Zotov, N., 2002. Element partitioning between immiscible borosilicate liquids: a high-temperature centrifuge study. Geochim. Cosmochim. Acta 66, 2603–2614. https://doi.org/10.1016/S0016-7037(02)00860-8.
Veksler, I.V., Dorfman, A.M., Dulski, P., Kamenetsky, V.S., Danyushevsky, L.V., Jeffries, T., Dingwell, D.B., 2012. Partitioning of elements between silicate melt and immiscible fluoride, chloride, carbonate, phosphate and sulfate melts, with implications to the origin of natrocarbonatite. Geochim. Cosmochim. Acta 79, 20–40. https://doi.org/10.1016/j.gca.2011.11.035.
Veksler, I.V., Dorfman, A.M., Kamenetsky, M., Dulski, P., Dingwell, D.B., 2005. Partitioning of lanthanides and Y between immiscible silicate and fluoride melts, fluorite and cryolite and the origin of the lanthanide tetrad effect in igneous rocks. Geochim. Cosmochim. Acta 69, 2847–2860. https://doi.org/10.1016/j.gca.2004.08.007.
Veksler, I.V., Kähn, J., Franz, G., Dingwell, D.B., 2010. Interfacial tension between immiscible liquids in the system K_2O-FeO-Fe_2O_3-Al_2O_3-SiO_2 and implications for the kinetics of silicate melt unmixing. Am. Mineral. 95, 1679–1685. https://doi.org/10.2138/am.2010.3456.
Watson, E.B., 1976. Two-liquid partition coefficients: experimental data and geochemical implications. Contrib. Mineral. Petrol. 56, 119–134. https://doi.org/10.1007/BF00375424.
Webster, J.D., Thomas, R., Veksler, I., Rhede, D., Seltmann, R., Forster, H., 1998. Late-stage processes in P-or F-rich granitic magmas. Acta Univ. Carol. Geol. 42, 181–188.
Yang, L., van Hinsberg, V.J., Samson, I.M., 2018. A new method to deconvolute binary mixture in LA-ICP-MS analyses to quantify the composition of phases smaller than the laser spot size. J. Anal. At. Spectrom. 33, 1518–1528. https://doi.org/10.1039/C8JA00078F.